Sensors and Materials, Vol. 38, No. 3 (2026) 1637–1655
MYU Tokyo

S & M 4398

Finite Element Impact Analysis of Integrated Cranial–Brain–Cervical Model Developed Using Optical 3D Scanning Sensors

Guan-Woei Tseng,[1] Yi-Wen Ou,[2] Chien-Ming Chen,[3] Hsing-Hui Lintseng,[2] Huang-Nan Lin,[2] Guang-Miao Huang,[2] Re-Wen Wu,[4*] and Bo-Wun Huang[2*]

[1]Department of Physical Medicine and Rehabilitation, Kaoshiung Chang Gung Memorial Hospital
No. 123, Dapi Road, Niaosong District, Kaohsiung 833401, Taiwan
[2]Department of Mechanical Engineering, Cheng Shiu University
No. 840, Chengqing Rd., Niaosong Dist., Kaohsiung 833301, Taiwan
[3]Kaohsiung Municipal Wunshan Senior High School
No. 31, Da-pi Rd., Niaosong District, Kaohsiung City 83341, Taiwan
[4]Department of Orthopaedic Surgery, Kaohsiung Chang Gung Memorial Hospital
No. 123, Dapi Road, Niaosong District, Kaohsiung 833401, Taiwan

(Received January 28, 2026; accepted March 19, 2026)

Keywords: computational biomechanics, cranio-cervical dynamics, traumatic brain injury (TBI), in silico simulation, passive safety optimization

Traumatic impacts resulting from vehicular collisions, sports activities, occupational accidents, and falls frequently lead to severe injuries of the cranium, brain, and cervical spine, posing a significant global public health burden. Accurate injury prediction requires high-resolution anatomical modeling supported by advanced sensing technologies. In this paper, we presented a comprehensive biomechanical impact analysis using a high-fidelity integrated cranial–brain–cervical (CBC) finite element model, with particular emphasis on the application of optical sensor systems in model development. The CBC model was established through reverse engineering using the Breuckmann SmartSCAN 3D system, which integrates industrial-grade CMOS/CCD imaging sensors to capture high-precision surface geometry. A commercially available 3B Scientific C18 five-part brain anatomical model was digitized, and the reconstructed geometry was further refined on the basis of a prior validated modeling work. The sensor-acquired data ensured high spatial resolution and geometric fidelity, directly enhancing computational accuracy. Modal analysis was conducted to determine the fundamental natural frequencies and mode shapes, followed by impact simulations under both damped and undamped conditions. Injury severity was quantified using the head injury criterion (HIC), peak linear acceleration, and velocity in accordance with standards established by the National Highway Traffic Safety Administration. Simulated HIC and peak acceleration results showed strong agreement with published validation data, confirming the predictive reliability of the sensor-informed CBC model. The proposed framework demonstrates how advanced 3D optical sensing

*Corresponding author: e-mail: huangbw@gcloud.csu.edu.tw
https://doi.org/10.18494/SAM6231

ISSN 0914-4935

can support biomechanical modeling, injury assessment, and the sensor-integrated design of next-generation protective equipment.

1. Introduction

In contemporary urban environments, high population density and an emphasis on operational efficiency characterize daily life, leading to a heavy reliance on automobiles and motorcycles for transportation. In June 2023, the United States recorded approximately 1.4 million vehicle registrations and 22.2 million annual sales, encompassing both commercial and passenger vehicles.[1] However, this mobility carries significant risks; in 2019, road injuries accounted for 1.24 million deaths, ranking as the twelfth leading cause of mortality globally.[2] Given that head and neck injuries are the most prevalent outcomes in vehicular accidents, substantial research efforts have been directed toward human head biomechanics in recent years.

The head injury criterion (HIC) remains the most widely adopted standard for quantifying the probability of head injury resulting from impact. The European Commission's COST 327 report on motorcycle safety helmets identified critical injury mechanisms and established tolerance thresholds for cranial–brain–cervical (CBC) injuries.[3] Research indicates that moderate-to-severe head injuries are strongly correlated with peak acceleration and cumulative loading—the primary factors driving HIC values. Consequently, HIC is instrumental in assessing the safety of vehicles, personal protective equipment (PPE), and sporting gear.

Surrogate head models are standard tools in biomechanical studies for investigating skull, brain, and cervical spine injuries. Thompson-Bagshaw *et al.*[4] reviewed 18 key studies spanning 1972 to 2019 and concluded that further research is required to evaluate the effects of head constraints, loading regions, and impactor geometry. Utilizing the finite element (FE) method, Teng *et al.*[5] reconstructed head impacts using a model that integrated the skull, brainstem, and cerebrospinal fluid (CSF). Their study emphasized the importance of acceleration signal filtering to ensure reliable HIC values and examined the correlation between rigid-body and centroid-node HIC measurements. Similarly, Nellippallil *et al.*[6] proposed a framework for assessing occupant injury risks. This framework incorporates both the HIC, calculated over durations ranging from 15 ms (HIC_{15}) to 36 ms (HIC_{36}), and criteria for neck injury, where HIC_{15} represents the HIC calculated over a time interval not exceeding 15 ms, i.e., $(t_2 - t_1) \leq 0.015$ s. Similarly, HIC_{36} corresponds to a maximum time interval of 36 ms, i.e., $(t_2 - t_1) \leq 0.036$ s. Refer to Eq. (1) for the formulation.

Recent advancements have focused on material properties and internal brain deformation. Abdi *et al.*[7] employed a validated FE head model (FEHM) to compare viscoelastic brain material models and assess the influence of skull density on simulation outcomes. He *et al.*[8] further refined these simulations by integrating fiber tracts from diffusion tensor imaging into a host brain model, allowing for the numerical tracking of axonal deformation. This approach facilitates the prediction of fiber tract damage, offering a potential objective function for optimizing protective gear.

Operational factors and vehicle performance significantly influence injury severity. Lujána *et al.*[9] used simulated vehicle models to quantify head and neck injuries in frontal crashes where

drivers held the steering wheel with only one hand. To validate their simulation, they analyzed real-world National Highway Traffic Safety Administration (NHTSA) frontal collision test data from sedans utilizing Hybrid III 50th percentile male dummies, the standard crash test dummies used globally to represent an average adult American male in frontal automobile impact tests, focusing on head acceleration, forces, and torques along the *X*-, *Y*-, and *Z*-axes. Their results indicated that compared with the standard two-hand position, all one-hand scenarios showed an over 67% probability of sustaining Abbreviated Injury Scale (AIS) 2+ injuries, that is, injuries with an AIS score of 2 or higher, which corresponds to a severity level of 'Moderate' or worse, with the risk of skull fracture reaching 89–94%.

Furthermore, Viano[10] analyzed the results of New Car Assessment Program (NCAP) tests conducted at 35 mph on 13 vehicles, noting that vehicle deformation increased significantly with speed. For drivers, the average HIC was 1099 with a chest acceleration of 55.7 g; seven out of thirteen vehicles failed to meet Federal Motor Vehicle Safety Standard No. 208 (FMVSS 208) standards. For passengers, the average HIC was 1179 with a chest acceleration of 47.2 g, where seven out of thirteen vehicles also failed. Overall, only four out of thirteen vehicles (30.8%) satisfied the injury criteria for both the driver and passenger positions.

Li *et al.*[11] employed FE analysis to investigate head frequency response, utilizing wavelet analysis to discuss the limitations of time-domain metrics such as HIC. Wang *et al.*[12] validated a commercial FE head-neck complex and a multi-body (MB) pedestrian model, finding substantial differences in predicted kinematics and brain injury risk between HIC_{15} and deformation-based criteria. For collision modeling, Liu *et al.*[13] proposed a parametric front-end model for car-to-e-bike collisions, achieving over 80% precision in predicting HIC_{15} using decision tree models.

Other scholars have focused specifically on skull fractures using the Total Human Model for Safety (THUMS) and drop tests.[14–17] Wang *et al.*[18] combined MB systems (MBS) with Livermore Software Technology Corporation (LSTC) - DYNAmic 3D (LS-DYNA) FE simulations of the THUMS model to reconstruct car-to-pedestrian collisions. To address complex injury types among vulnerable road users, Han *et al.*[19] introduced the Head-Weighted Injury Criterion (HWIC4), integrating HIC_{15}, angular acceleration, coup pressure, and maximum principal strain (MPS).

Beyond traditional HIC, researchers have focused on specific brain injury criteria.[20,21] Östh *et al.*[22] evaluated kinematics from 221 frontal and side crash tests and concluded that mass-spring-damper models, specifically Diffuse Axonal Multi-Axis General Evaluation (DAMAGE) and Convolution of Impulse response for Brain Injury Criterion (CIBIC), were superior in capturing MPS for both the Test Device for Human Occupant Restraint (THOR) and Worldwide Harmonized Side Impact Dummy (WorldSID) datasets.

In protective equipment studies, such as those by Zheng *et al.*,[23] the biomechanical responses of helmeted heads under various impact conditions have been investigated. Rodriguez-Millan *et al.*[24] evaluated helmet pad systems against ballistic threats using a Hybrid III dummy. Their findings showed that thicker polyurethane foams and honeycomb pads significantly reduced brain injury risk, as indicated by the Peak Linear Acceleration (PLA), the Wayne State Concussion Tolerance Curve (WSTC), and HIC values, without risk of cervical injury.

Finally, to manage computational complexity, researchers have explored mesh reduction. Margulies and Thibault[25] used idealized FE models to demonstrate the influence of skull and suture structures on biomechanical responses, while Carmo *et al.*[26] discussed the optimization of mesh size for the skull, brain, and CSF in a female FEHM (FeFEHM).

In this research, we developed an integrated CBC model utilizing the FE method. The authors analyzed biomechanical impacts on the CBC model to obtain HIC, acceleration, and velocity data, aiming to enhance injury mitigation strategies.

2. Data, Materials, and Methods

2.1 Role of high-resolution optical sensing in model development

The geometric fidelity of our integrated CBC model is entirely dependent on the advanced sensor technology employed. We now explicitly highlight that the industrial-grade CMOS/CCD sensor array in the Breuckmann SmartSCAN 3D system, with its sub-millimeter accuracy (±0.01 mm), was not merely a data acquisition tool, but the essential enabler for capturing the complex, subject-specific topography of the cranial, brain, and cervical structures. This level of detail is a prerequisite for creating a predictive FE model capable of resolving the localized strains and stresses that are critical for injury prediction.

The geometric architecture of the integrated CBC model was acquired using a white-light optical three-dimensional scanning system (Breuckmann SmartSCAN 3D). This system utilizes industrial-grade CMOS sensors with a high-resolution CCD camera array to capture detailed surface topography (accuracy up to ±0.01 mm). To ensure the fidelity of the subsequent FE analysis, the raw scanning data underwent rigorous multistage geometric processing. Initially, the acquired point cloud data were filtered to reduce the high-frequency noise inherent in optical scanning while preserving critical anatomical features. The denoised point clouds from multiple scanning angles were then registered and merged using an iterative closest point (ICP) algorithm to reconstruct a seamless, watertight polygonal mesh representing the outer surfaces of the cranial, brain, and cervical structures.

2.2 Research process

Reverse engineering was employed to reconstruct the CBC geometry, which was subsequently smoothed and imported into SolidWorks CAD software to establish the computational model. FE analyses were then performed using ANSYS Workbench to investigate the dynamic characteristics of the human head. Mesh convergence was evaluated using the fundamental natural frequency. After convergence was achieved, modal and impact analyses were conducted under both damped and undamped conditions.

For the impact analysis, a curve-fitting approach was applied to obtain a continuous acceleration–time function. The HIC was calculated by the time-domain integration of the derived acceleration function and assessed with reference to international safety standards. HIC quantifies the risk of head injury. A lower HIC value indicates a lower risk. U.S. safety standard FMVSS 201 requires interior parts such as pillars to have a HIC(d) value below 1000. The

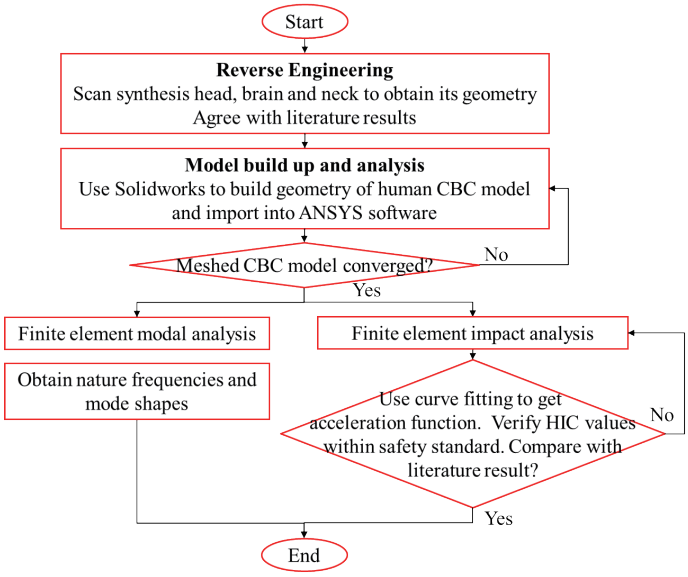

Fig. 1. (Color online) Flowchart of the research process.

simulated acceleration responses and corresponding HIC values were further validated through comparison with previously published results. An overview of the complete research workflow is presented in Fig. 1.

2.3 CBC modeling, convergence, and modal analysis

The human head model employed in this study was developed on the basis of contemporary anatomical and physiological data,[27] as illustrated in Fig. 2. The structural CBC model consisted of the cranium, cervical vertebrae, brain tissue, and CSF. A sensor-based optical 3D scanning system (Breuckmann SmartSCAN 3D) was used to digitize a Classic 5-Part Brain (C18) anatomical model manufactured by 3B Scientific Corporation. The acquired surface data were subsequently processed and reconstructed into a three-dimensional CAD model using SolidWorks software.

To improve computational efficiency, simplified modeling approaches were considered, as the feasibility of reduced-degree-of-freedom (DoF) (2- or 3-DoF) kinematic models for head dynamics analysis has been demonstrated in previous studies.[28,29] In the present CBC model, the human brain geometry based on the model proposed by Tseng *et al.* was adopted.[30] Prior FE analyses have shown that the dynamic responses of simplified brain models are in good agreement with those of more anatomically detailed models incorporating cerebral sulci, supporting the validity of the adopted modeling strategy.

The assembled 3D head–neck model was imported into ANSYS Workbench for dynamic characteristic analysis. In this simulation, the skull, cervical vertebrae, and brain tissues were discretized using 3D 10-node tetrahedral Solid187 elements, whereas the CSF was modeled with 3D 20-node hexahedral Solid186 elements.[31] These higher-order elements were specifically

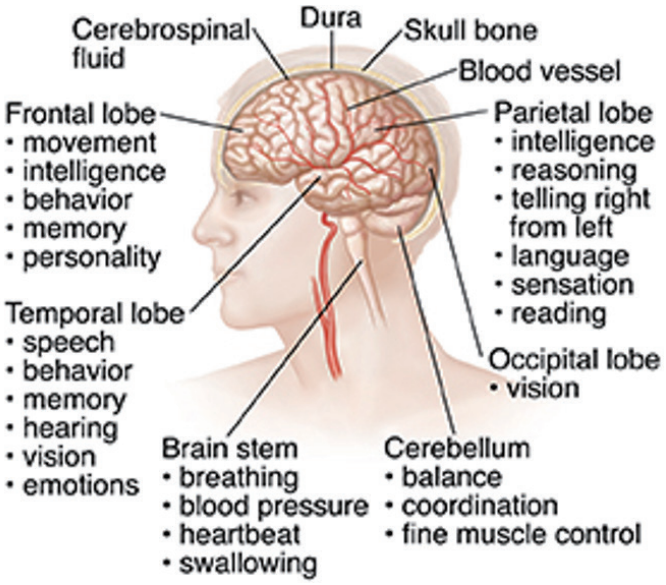

Fig. 2. (Color online) Anatomical schematic of the human cranial and cerebral structures.[27]

chosen for their superior ability to represent complex, irregular geometries without the loss of accuracy typically associated with unstructured grids.

Utilizing ANSYS's advanced meshing algorithms, the model's structural integrity was maintained through a refined discretization strategy. Since the mesh density and element morphology directly dictate the computational coarseness and the subsequent precision of the analysis, the grid size was optimized to balance numerical stability with result accuracy. The finalized FE meshes for the skull–neck complex, brain tissue, and CSF are illustrated in Fig. 3. The influence of the structural viscous damping coefficient on internal brain tissue damage is a critical consideration in traumatic biomechanics. Chafi *et al.*[32] characterized the CSF as a fluid-like, viscoelastic, and nearly incompressible medium, characterized by a low shear modulus and a high bulk modulus. To account for the damping properties of brain tissue, the viscous damping coefficient (β) was estimated using established constitutive formulations. Empirical findings indicate that the β boundary ranges from 0.67 to 0.87% within a frequency spectrum of 65 to 350 Hz, while a baseline β value of 0.001 is typically assigned to both the brain and the skull. Following this methodology, in this study, we investigated the comparative biomechanical responses of the integrated CBC model under both damped and undamped conditions to evaluate the energy dissipation effects during impact.

The fundamental material parameters defined in this study include Young's modulus, bulk modulus, Poisson's ratio, density, and viscosity. These values were assigned referring to the established biomechanical properties for the human skull, cervical vertebrae, brain tissue, and CSF, as detailed in Table 1. Regarding boundary conditions, the model was rigidly clamped at the seventh cervical vertebra (C7), which serves as the anatomical junction between the cervical and thoracic regions. This fixed boundary condition, illustrated in Fig. 4, was implemented by constraining all translational degrees of freedom ($U_x = U_y = U_z = 0$) at the C7 interface, while all

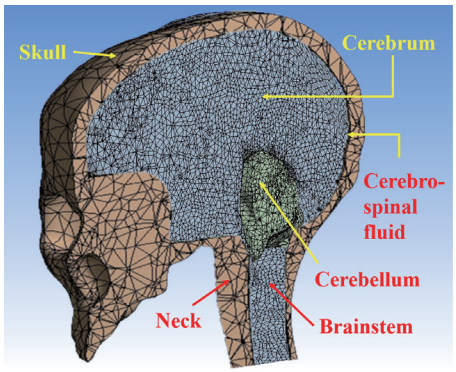

Fig. 3. (Color online) FE mesh of the integrated human CBC model.

Table 1
Material properties of the integrated human CBC model.[33–35]

Components	Young's modulus (MPa)	Bulk modulus (MPa)	Poisson's ratio v	Density (kg/m^3)	Viscosity (Pa·s)
Skull	16500	—	0.25	2132.6	—
Neck bone	2500	—	0.25	2132.6	—
Brain tissue	0.25	2190	0.48	1007	—
CSF	0.145	2190	0.49	1040	0.001

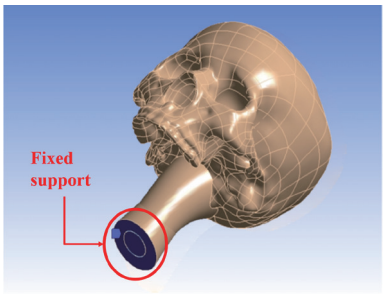

Fig. 4. (Color online) Boundary conditions of the human CBC model: fixed at the seventh cervical vertebra (C7) and free elsewhere.

other regions remained free to respond to dynamic loading. To ensure numerical stability, convergence analysis was performed using various ANSYS solvers. This iterative process involved systematically increasing the mesh density to monitor the stability of the fundamental natural frequency. Convergence was considered achieved when fluctuations in the natural frequency became negligible, thereby determining the optimal element count for subsequent modal and impact simulations. Furthermore, this computational framework allowed for the extraction of multiple natural frequencies and their corresponding kinematic parameters, including amplitude, displacement, velocity, and acceleration profiles.

2.4 Impact analysis

In this section, the details of the impact dynamic simulations performed on the converged integrated human CBC model are given. A nonlinear transient structural dynamic module within ANSYS Workbench was utilized to simulate the biomechanical response of the head under impulsive loading. The impact force-time histories were defined between 7000 and 10000 N, with durations ranging from 0.001 to 0.01 s. A representative transient force profile is illustrated in Fig. 5. The impact was localized at the frontal region of the skull along the *Z*-axis, concentrated over an effective area of approximately 860 mm^2, as depicted in Fig. 6. To observe the vibrational response of the internal brain tissue, various impact magnitudes were applied to the external cranium. The resulting temporal variations in brain displacement and kinematic response were evaluated against established safety criteria. Specifically, PLA (G_{max}) and HIC values derived from the impacted model were employed to quantify the severity of the head injury. In this study, the HIC36 index was implemented to validate the feasibility of the data obtained from the head–neck FE analysis. This criterion, part of FMVSS 208, was originally

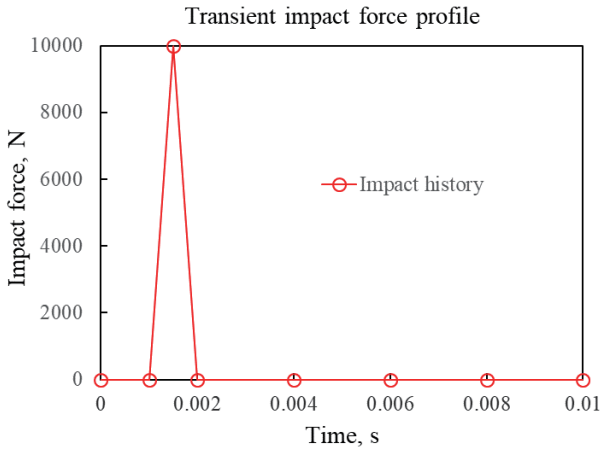

Fig. 5. (Color online) Transient impact force profile acting on the human CBC model.

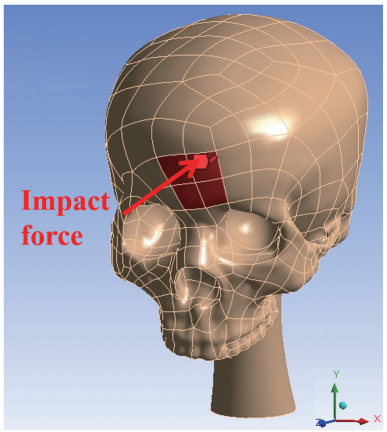

Fig. 6. (Color online) Schematic of the impact loading area on the frontal region of the CBC model.

adopted by NHTSA in 1993, with comprehensive updates announced in 2019.[36] Ensuring the reliability of these simulated metrics is essential before the computational framework can be extended to evaluate the dynamic protective characteristics of motorcycle helmets.

2.5 Evaluation and verification of HIC

In this study, a comprehensive impact dynamic analysis was conducted using the integrated human CBC model. To enhance the reliability of the FE model beyond simulation-based damage assessment, the numerical results were validated against experimental data obtained from established literature. The resultant acceleration components along the *X*-, *Y*-, and *Z*-axes were extracted and processed using DeltaGraph and Microsoft Excel to generate a continuous, curve-fitted acceleration function, $a(t)$. As both analytical tools yielded identical governing equations, Microsoft Excel was utilized to perform the mathematical computations and determine the coefficient of determination (R^2) to ensure the reliability of fit. The *HIC* value, as specified by the U.S. FMVSS 208 regulations, was calculated by integrating the acceleration function as in Eq. (1). A representative curve-fitted acceleration profile is illustrated in Fig. 7. The *HIC* value derived from this integration serves as the standard metric for quantifying traumatic brain injury (TBI) severity and can be directly correlated with vehicle dynamic testing data. In accordance with the HIC36 protocol, a threshold value of less than 1000 is adopted as the primary safety standard for human head protection.

$$HIC = \max\left[\frac{1}{t_2 - t_1}\int_{t_1}^{t_2} a(t)dt\right]^{2.5}(t_2 - t_1) \tag{1}$$

The analytical framework of this research is organized into three distinct stages to facilitate a comprehensive biomechanical evaluation.

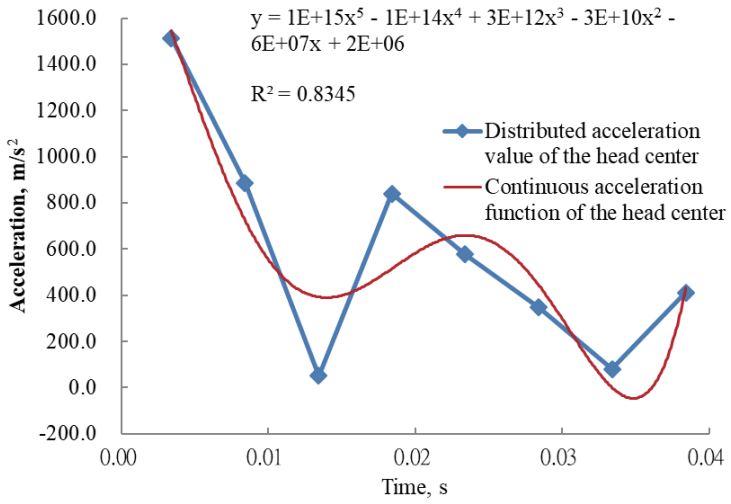

Fig. 7. (Color online) Curve-fitted acceleration function and the corresponding coefficient of determination (R^2) for the impacted CBC model.

1) Temporal Sensitivity and Damping Analysis: The first stage is the evaluation of the dynamic impact response under a constant force across varying durations. A comparative study is conducted between damped and undamped head models to quantify the energy dissipation effect of the structural viscous damping coefficient.
2) Force Magnitude and Injury Assessment: The second stage is the investigation of the influence of varying impact magnitudes under a constant time duration. PLA and HIC values are employed as the primary assessment metrics to determine whether the biomechanical response exceeds the threshold for severe TBI.
3) Model Validation: The final stage establishes the feasibility and accuracy of the proposed FE model. By replicating the initial and boundary conditions from established literature, the simulation results are cross-referenced with experimental benchmarks to verify the model's predictive reliability.

3. Results

3.1 FE convergence and modal analysis

A mesh convergence study was performed on the integrated human head model to ensure the numerical stability and accuracy of the simulation. Following the determination of the optimal element size, subsequent dynamic analyses were conducted to validate the predictive reliability of the discretized model. As illustrated in Fig. 8, the fundamental natural frequency of the head model stabilized at 66.46 Hz as the element count increased. Convergence was effectively achieved at approximately 400000 elements; consequently, a mesh density of 450000 elements was selected for all subsequent modal and impact simulations to ensure high-fidelity results.

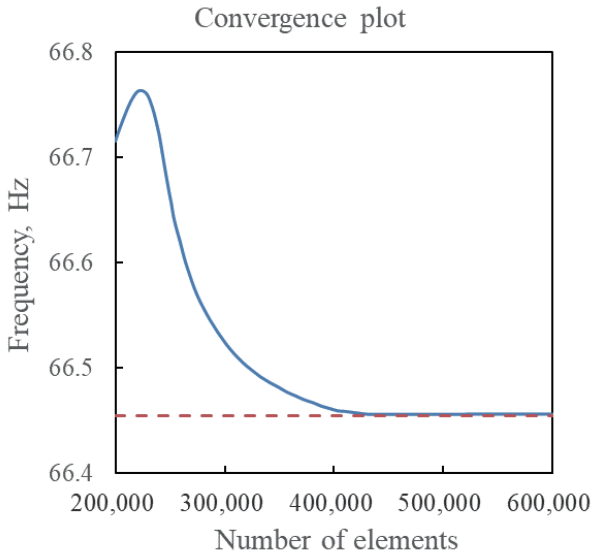

Fig. 8. (Color online) Mesh convergence analysis based on fundamental natural frequency.

Table 2
First six natural frequencies of the CBC model obtained from modal analysis.

Mode number	Natural frequency (Hz)
1	66.46
2	73.31
3	102.67
4	112.76
5	115.17
6	129.94

The modal analysis revealed the inherent dynamic characteristics of the CBC structure. From the converged model, the first natural vibration frequency was confirmed to be 66.46 Hz. Table 2 summarizes the first six natural frequencies derived from the FE modal analysis, providing a comprehensive overview of the vibrational modes of the overall human CBC model.

3.2 Influence of impact duration on HIC, peak acceleration, and velocity

In this section, the impact force was fixed at 7000 N while the duration was varied from 0.001 to 0.01 s to evaluate the temporal sensitivity of the CBC model. A comparative analysis was performed to determine the effect of the viscous damping coefficient (β). While a standard impact range of 7000–8000 N is suggested in the literature, the impact duration is often a more elusive variable in real-world scenarios. Consequently, the temporal range was expanded to precisely capture the acceleration and velocity responses at the model's center of mass and to identify the critical duration that maximizes the HIC value. Raw acceleration data from ANSYS Workbench (originally in mm/s^2) were converted to standard gravitational units (G) and m/s^2 for further analysis. We first analyzed the undamped case ($\beta = 0$) to establish a baseline, followed by the damped case ($\beta = 0.001$). HIC values were derived via Eq. (1) using the extracted acceleration–time histories. The results, illustrated in Fig. 9, indicate that a 6 ms impact duration represents the most critical threshold for head injury. For the undamped structure, this duration resulted in a peak acceleration of 140.61 m/s^2 and a substantial HIC value of 1995.84. Conversely, incorporating a damping coefficient of 0.001 reduced the peak acceleration to 83.83 m/s^2 and the HIC to 345.92, demonstrating the vital role of damping in injury mitigation. Observations reveal that the maximum HIC (blue line) does not temporally coincide with the peak acceleration (green line). Because the HIC is an integral-based metric, it accounts for the cumulative energy transfer over time; thus, the HIC peak is characteristically delayed relative to the peak acceleration. Furthermore, Fig. 10 displays the relationship between maximum velocity and HIC. While the HIC trends remain consistent with those in Fig. 9, the damped velocity curve (purple line) is significantly attenuated compared with the undamped profile (green line), further validating that structural damping effectively dissipates impact energy.

3.3 Influence of impact force magnitude on HIC, peak acceleration, and velocity

In this stage of the simulation, the impact duration was held constant at 10 ms, while the impact force magnitude was varied from 1000 to 10000 N. The primary objective was to

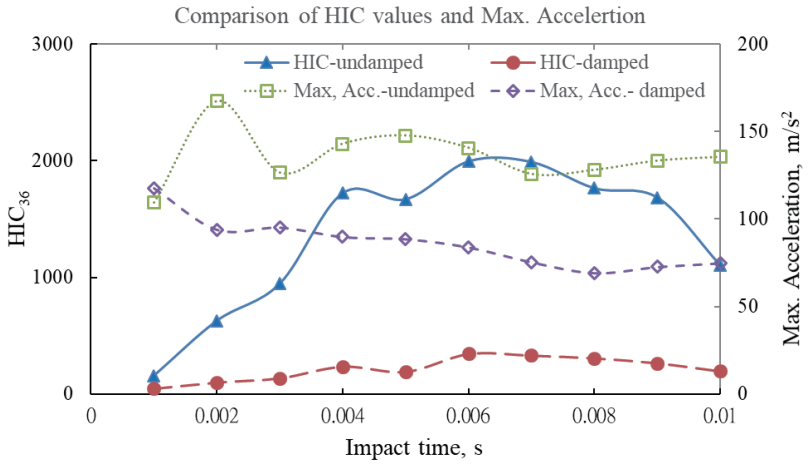

Fig. 9. (Color online) HIC values and peak accelerations across varying impact durations under damped and undamped conditions.

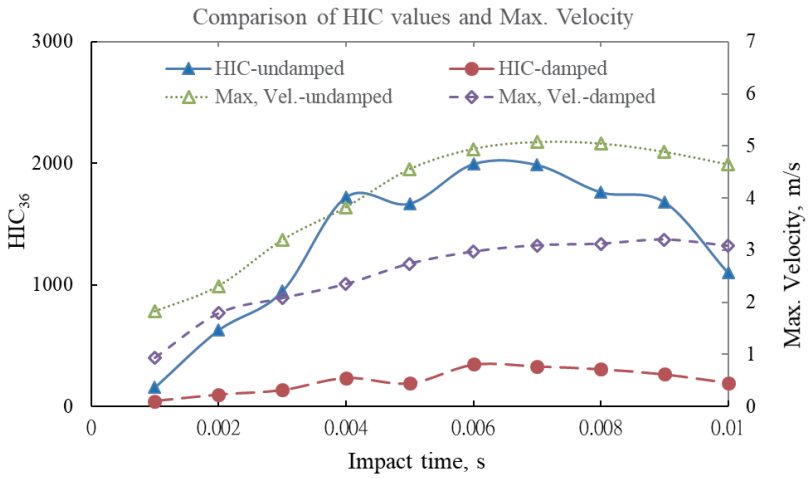

Fig. 10. (Color online) HIC values and peak velocities for various impact durations under damped and undamped conditions.

investigate the acceleration response at the head model's center of mass and determine the correlation between force magnitude and HIC value. Dynamic impact simulations were performed for both undamped ($\beta = 0$) and damped ($\beta = 0.001$) configurations. Kinematic data, including velocity and acceleration, were extracted to compute the HIC values via integration of the acceleration–time histories. As illustrated in Fig. 11, the maximum acceleration (G) experienced by the CBC model exhibits a linear correlation with the applied impact force. Furthermore, the injury severity is intrinsically linked to the impact energy, represented by the area under the acceleration–time curve. For both damped and undamped cases, HIC and peak acceleration increased monotonically with force. For instance, upon a 10000 N impact, the undamped HIC and acceleration reached 3527.3 and 193.2 m/s^2, respectively. However, with the application of a 0.001 damping coefficient, these values were significantly attenuated to 999.8

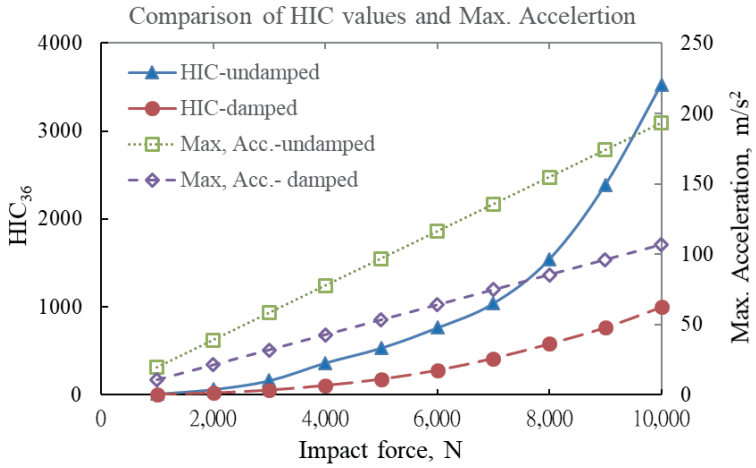

Fig. 11. (Color online) HIC and peak acceleration as functions of impact force magnitude under damped and undamped conditions.

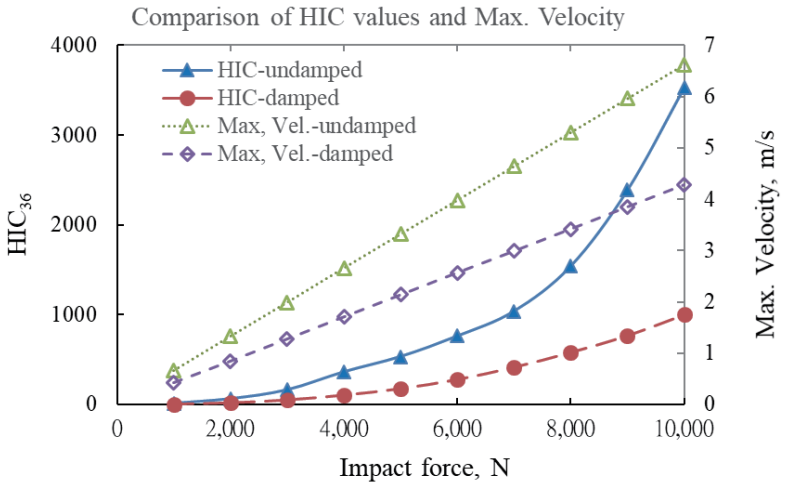

Fig. 12. (Color online) HIC and peak velocity as functions of impact force magnitude under damped and undamped conditions.

(HIC) and 106.8 m/s^2 (acceleration). These results demonstrate that structural damping effectively dissipates impulsive energy, thereby mitigating the risk of TBI—a principle that can be further enhanced through the use of protective helmets. Conversely, Fig. 12 highlights the relationship between maximum velocity and HIC across the varying force spectrum. The results indicate that the peak velocity attained by the CBC model is directly proportional to both the impact force and the peak acceleration. Under constant force conditions, the velocity at the model's center of mass scales linearly with the acceleration profile. At the maximum load of 10000 N, the peak velocity decreases from 6.62 m/s in the undamped scenario to 4.28 m/s in the

damped case. This consistent reduction in kinematic response across all force levels underscores the importance of incorporating damping characteristics in the design of head protection systems and reducing the risk of TBI.

4. Discussion

Several points are discussed separately below.

4.1 Validation by comparison with literature results

To validate the proposed FE model, the initial and boundary conditions from previous literature were replicated in the current simulation framework. Specifically, in this study, the authors adopted the impact conditions established by Nahum, as cited by Chinn *et al.*,[3] to ensure a standardized benchmark for comparison. Assuming an undamped condition ($\beta = 0$) consistent with the reference study, the resulting acceleration waveform from the current CBC model (red line) exhibited a strong correlation with the results reported by Chinn *et al.* (blue line), as illustrated in Fig. 13. The inset graph in the upper-right corner of Fig. 13 provides an expanded view of the acceleration response over a 15 ms interval to enable a detailed comparison. An analysis of the acceleration profiles at the model's center of mass reveals significant similarities in peak magnitude, waveform symmetry, and overall temporal distribution. Quantitatively, the experimental benchmarks from Chinn *et al.*[3] were compared against the numerical data in this study, as summarized in Table 3. The relative errors for maximum acceleration and the HIC value were approximately 27.5 and 23.8%, respectively. Despite these

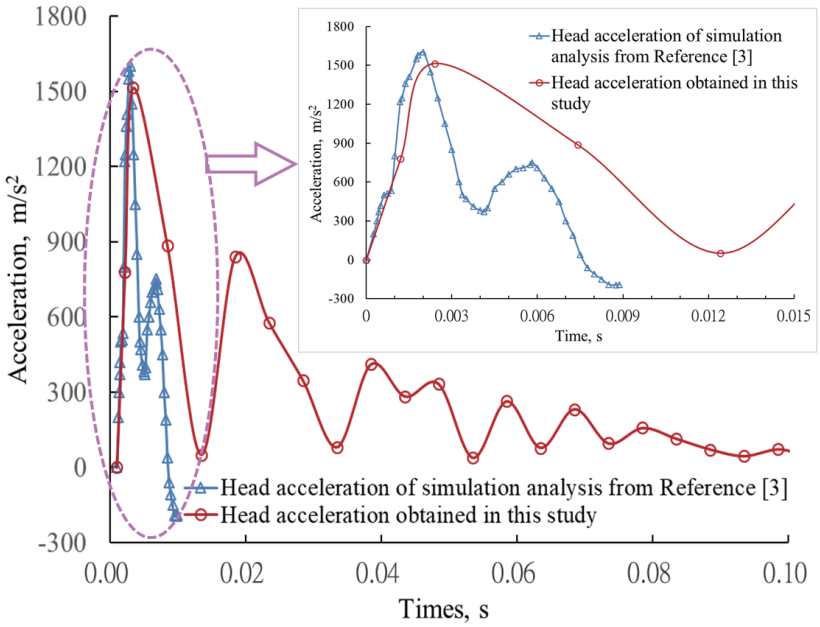

Fig. 13. (Color online) Head center-of-mass acceleration following impact obtained in the current study and simulated by Chinn *et al.*[3]

Table 3
Peak acceleration and HIC values obtained in the current study and by Chinn *et al.*[3] under a 6900 N impact force.

Item	This study (A)	Chinn *et al.*[3] (B)	Relative error |((A)−(B))/(B)|
Maximum acceleration (m/s^2)	143.5	198	27.5%
HIC value	921	744	23.8%

variances, the simulation successfully captured the fundamental kinematic trends observed in the experimental data. Consequently, these results confirm that the developed integrated CBC model is a valid and robust tool for predicting head injury kinematics, providing a reliable foundation for future research into the optimization of protective headgear.

Teng *et al.*[5] specified the appropriate filtering class for acceleration signals used in HIC calculations and conducted a quantitative comparison between rigid body HIC and centroid node HIC. In their study, a head acceleration of 20 g (approximately 196 m/s^2) was obtained from rigid body motion (RBM) analysis. For the SAE channel class of 900 Hz, the reported HIC values under the frontal RBM condition were 955, 590, 350, and 210 for impact velocities of 40, 45, 50, and 55 m/s, respectively. The maximum acceleration and HIC values obtained in the present study and the results reported by Teng *et al.* are summarized in Table 4. The relative errors in maximum acceleration and HIC were approximately 26.8 and 3.6%, respectively, demonstrating good agreement in HIC prediction despite a moderate deviation in peak acceleration.

Overall, the present results demonstrate good agreement with previously published data, including those reported by Chinn *et al.*[3] and Teng *et al.*,[5] thereby supporting the validity and reliability of the proposed model.

4.2 Limitations of this study

1) Simplified anatomical representation and material assumptions
   Although the integrated CBC FE model captures the overall structural configuration of the head–neck system, several anatomical details and tissue heterogeneities were simplified to reduce computational complexity. The material properties of biological tissues were assumed to be homogeneous and isotropic, which may not fully reflect the nonlinear and viscoelastic behavior observed in real human tissues under high-rate impact conditions.
2) Limited validation scope and loading scenarios
   Model validation was primarily conducted through comparison with previously reported simulation and experimental data in the literature, rather than direct subject-specific experimental measurements. In addition, the impact simulations were restricted to a limited set of loading directions, velocities, and boundary conditions. Consequently, the findings may not fully represent the variability of real-world impact scenarios involving complex multidirectional forces and individual anatomical differences.

Table 4
Peak acceleration and HIC values obtained in the present study and by Teng *et al.*[5]

Item	This study (A)	Teng *et al.*[5] (C)	Relative error |((A)−(C))/(C)|
Maximum acceleration (m/s^2)	143.5	196	26.8%
HIC value	921	955	3.6%

4.3 Implications for sensor technology and materials

The true value of our *in silico* CBC model lies in its application as a platform for developing and testing new sensor technologies. A high-fidelity biomechanical model is essential for virtually prototyping and validating "smart" protective equipment.

The following is an outline of how our model can be used

1) Optimize Sensor Placement:
   Simulate impacts to determine optimal locations for embedding pressure, strain, or accelerometer sensors within helmets or other protective gear to maximize data capture on head kinematics.
2) Virtually Prototype Sensor-integrated Materials:
   The model provides a testbed for evaluating the performance of novel sensor materials (e.g., flexible piezoresistive films and optical fibers) by simulating how their presence affects both the sensor reading and the structural integrity of the protective equipment.
3) Establish Sensor-output-to-injury Correlations:
   By correlating simulated sensor readings (e.g., from a virtual accelerometer) with predicted tissue-level injury metrics (such as HIC and peak strain), our framework helps define the performance specifications required for new sensors to be clinically relevant.

4.4 Future work

While the utility of high-resolution CMOS/CCD optical sensors for generating high-fidelity geometric models was successfully demonstrated in this study, the next logical advancement involves transitioning from offline modeling to *in situ* impact sensing. Future work will be focused on the development of a miniaturized, flexible hybrid sensor array designed for direct integration into protective headgear (e.g., helmets).

Current HIC calculations rely on post-impact analysis or rigid, laboratory-bound accelerometers. We propose a novel sensing layer composed of flexible MEMS accelerometers and piezoresistive thin-film pressure sensors embedded within the liner of a helmet. Unlike the Breuckmann system used for geometric acquisition, these sensors would capture real-time linear acceleration and deformation data at the interface between the head and the protective equipment during an impact event.

The high-fidelity cranial geometry acquired via the Breuckmann SmartSCAN 3D system will serve as the anatomical baseline for calibrating this sensor network. By mapping the sensor positions onto the detailed digital twin established in this study, we can correlate localized strain data from the sensors with the global HIC values predicted by our FE model.

The proposed sensor suite will target the following.

1) High-bandwidth MEMS accelerometers (range: ±500 to ±2000 g) to capture the brief, intense acceleration peaks critical for HIC calculation (HIC_{15} and HIC_{36}).

2) Flexible piezoresistive films to detect skull deformation and liner compression, providing a secondary data stream for validating neck injury criteria.
3) Low-power wireless data transmission for real-time telemetry in high-risk environments (e.g., contact sports, construction sites).

5. Conclusions

In this study, we developed a high-fidelity FE model of the human head, incorporating realistic biomechanical material properties to simulate the dynamic response of the skull, brain tissue, and CSF. By employing modal and impact dynamic analyses, we evaluated head injury severity on the basis of HIC_{36} and peak resultant acceleration, as stipulated by the FMVSS. The primary findings are summarized as follows.

1) The application of CMOS/CCD image sensors in a white-light optical scanning system is essential for capturing the geometry of the CBC structure.
2) Injury Assessment and HIC Standards: The impact dynamic analysis successfully captured the triaxial resultant acceleration at the head's center of gravity. Under the current safety threshold defined by NHTSA, the calculated HIC_{36} values serve as a reliable indicator for assessing the risk of TBI, with 1000 being the critical limit for safety compliance.
3) Loading Parameters and Energy Transfer: The results demonstrate that the severity of head injury is not solely dependent on peak acceleration, but is also a function of the impact energy, represented by the area under the acceleration–time curve. This underscores the importance of pulse duration and loading history in crash-worthiness analysis.
4) Model Validation: A comparative analysis showed that the acceleration waveforms, peak amplitudes, and symmetry trends generated by this model are highly consistent with established results of domestic and international research. This alignment validates the structural integrity and numerical accuracy of the proposed FE model for future biomechanical applications.
5) Critical Role of Viscous Damping: The inclusion of viscous damping coefficients within the head model is crucial for simulating the energy-dissipating characteristics of biological tissues. The results indicate that viscosity significantly mitigates impact forces and buffers the brain against rapid displacement. Conversely, as impact force increases, the diminishing relative effect of damping leads to a sharp rise in HIC values, escalating the risk of catastrophic cranial damage.

In conclusion, the novelty of this study lies in the synergistic integration of high-precision optical sensing with a robust computational framework for head impact analysis. By leveraging industrial-grade CMOS sensors and a high-resolution CCD camera array to capture detailed surface topography, the developed CBC model provides a geometrically accurate foundation for simulation. The key finding of this work delineates the fundamental interplay between material viscosity and impact energy, a critical insight for advancing next-generation head protection systems in automotive and sports safety. The validity of the proposed framework was further confirmed by the strong quantitative agreement between the simulation results and the results of two benchmark studies in the literature. Building on the future directions outlined above, this work lays the groundwork for transforming passive protective equipment into active, sensor-integrated safety systems. By embedding sensing capabilities directly into the material

architecture, we can extend beyond laboratory simulations to enable real-world impact monitoring. Such a sensor system would allow for the immediate, on-site calculation of HIC and the prompt diagnosis of potential traumatic brain injuries, effectively bridging the gap between advanced biomechanical modeling and practical, life-saving technology.

Acknowledgments

This research was funded by the National Science and Technology Council, Taiwan, R.O.C., NSTC 114-2622-8-006-014-NSB.

References

1 Vehicle registrations – United States. June of 2023. https://countryeconomy.com/business/car-registrations/usa
2 H. Ritchie, F. Spooner, and M. Roser: Causes of Death. OurWorldInData.org., 2019. Retrieved from: https://ourworldindata.org/causes-of-death (Online Resource).
3 B. Chinn, B. Canaple, S. Derler, D. Doyle, D. Otte, E. Schuller, and R. Willinger: COST 327 Motorcycle Safety Helmets, Final Report of the Action, European Commission Directorate General for Energy and Transport, 2001.
4 D. W. Thompson-Bagshaw, R. D. Quarrington, and C. F. Jones: Ann. Biomed. Eng. **50** (2022) 1750.
5 D. Teng, Z. Chen, Z. Wu, Y. Zhang, B. Yang, L. Tang, Z. Jiang, Y. Liu, Z. Liu, and L. Zhou: Injury **55** (2024) 111457.
6 A. B. Nellippallil, P. R. Berthelson, L. Peterson, and R. K. Prabhu: Multiscale Biomechanical Modeling of the Brain, R. Prabhu and M. Horstemeyer Eds. (Academic Press, 2022) pp. 153–176.
7 H. Abdi, D. Sánchez-Molina, S. García-Vilana, and V. Rahimi-Movaghar: Heliyon **10** (2024) e29427.
8 G. He, L. Fan, and M. F. Horstemeyer: Comput. Biol. Med. **181** (2024) 109063.
9 K. V. P. Lujána, R. C. Silva, A. B. S. Oliveira, D. A. L. Cordoba, P. V. Muterlle, J. A. Araújo, J. L. A. Ferreira, and C. R. M. Silva: Lat. Am. J. Solids Struct. **18** (2021) e336.
10 D. C. Viano: Traffic Inj. Prev. **25** (2024) 288.
11 G. Li, S. k. Xu, T. Xiong, K. Li, and J. Qiu: Front. Bioeng. Biotechnol. **12** (2024). https://doi.org/10.3389/fbioe.2024.1364741
12 F. Wang, C. Yu, B. Wang, G. Li, K. Miller, and A. Wittek: Traffic Inj. Prev. **21** (2020) 102.
13 Y. Liu, X. Wan, W. Xu, L. Shi, Z. Bai, and F. Wang: Accid. Anal. Prev. **168** (2022) 106599.
14 D. Sahoo, C. Deck, N. Yoganandan, and R. Willinger: J. Mech. Behav. Biomed. Mater. **57** (2016) 24. https://doi.org/10.1016/j.jmbbm.2015.11.014
15 D. E. Krzeminski, F. K. Fuss, Y. Weizman, A. Ketabi, and S. G. Piland: Procedia Eng. **112** (2015) 190.
16 A. M. Loyd, R. W. Nightingale, J. F. Luck, C. D. Bass, H. C. Cutcliffe, and B. S. Myers: J. Biomech. **93** (2019) 167.
17 F. Wang, Z. Wang, L. Hu, H. Xu, C. Yu, and F. Li: Front. Bioeng. Biotechnol. **9** (2021) 677982.
18 J. Wang, Z. D. Li, F. Ying, D. H. Zou, and Y. Chen: J. Forensic Legal Med. **91** (2022) 102433.
19 Y. Han, H. Wu, D. Pan, L. Su, L. Shi, and F. Wang: J. Biomech. **165** (2024) 112024.
20 X. Zhan, Y. Li, Y. Liu, A. G. Domel, H. V. Alizadeh, S. J. Raymond, K. Ruan, S. Barbat, S. Tiernan, O. Gevaert, M. M. Zeineh, G. A. Grant, and D. A. Camarillo: J. R. Soc. Interface **18** (2021) 20210260.
21 D. Sahoo, F. Coulongeat, F. Fuerst, and G. Marini: IRCOBI Conf. Proc. Munich, Germany, 2021, IRC-20-63, 529–542.
22 J. Östh, K. Bohman, and L. Jakobsson: Traffic Inj. Prev. **24** (2023) 56.
23 G. Zheng, X. Zhang, S. Li, T. Pang, and Q. Li, G. Sun: Compos. Struct. **291** (2022) 115514.
24 M. Rodriguez-Millan, I. Rubio, F. J. Burpo, A. Olmedo, J. A. Loya, K. K. Parker, and M. H. Miguélez: Int. J. Impact Eng. **181** (2023) 104757.
25 S. S. Margulies and K. K. Thibault: J. Biomech. Eng. **122** (2000) 364. https://doi.org/10.1115/1.1287160
26 G. P. Carmo, M. Dymek, M. Ptak, R. J. Alves-de-Sousa, and F. A. O. Fernandes: Comput. Methods Programs Biomed. **231** (2023) 107430.
27 Anatomy of the Brain, Saint Luke's: https://www.saintlukeskc.org/health-library/anatomy-brain (accessed on 12 March 2021).

28 K. Laksari, L. C. Wu, M. Kurt, C. Kuo, and D. C. Camarillo: J. R. Soc. Interface **12** (2015) 20150331. https://doi.org/10.1098/rsif.2015.0331
29 Z. Taha, M. H. A. Hassan, and I. Hasanuddin: Sadhana **40** (2015) 1567.
30 J.-G. Tseng, B.-W. Huang, Y.-W. Ou, K.-T. Yen, and Y.-T Wu: Bioengineered **7** (2016) 219.
31 ANSYS Workbench User's Guide, ANSYS Inc., Canonsberg, PA, USA, January 2023 R1.
32 M. S. Chafi, V. Dirisala, G. Karami, and M. Ziejewski: Proc. Ins. Mech. Eng. H: J. Eng. Med. **223** (2009) 1003. https://doi.org/10.1243/09544119JEIM631
33 Y. Luo, Z. Li, and H. Chen: Proc. Inst. Mech. Eng. H: J. Eng. Med. **226** (2012) 499.
34 A. A. Linninger, K. Tangen, C. Y. Hsu, and D. Frim: Annu. Rev. Fluid Mech. **48** (2016) 219.
35 G. Cardillo and C. Camporeale: J. Fluids Struct. **102** (2021) 103251.
36 FMVSS 208, Occupant Crash Protection, Federal Motor Vehicle Safety Standard, Washington, U.S.A., 1993. (Updated rulemaking is announced at September 27, 2019)